Springer

KSME

Journal of Mechanical Science and Technology 33 (1) (2019) 279~288
www.springerlink.com/content/1738-494x(Print)/1976-3824(Online)
DOI 10.1007/s12206-018-1227-0

Analysis of flow transition and separation on oscillating airfoil by pressure signature †

Binbin Wei, Yongwei Gao*, Long Wang and Dong Li

School of Aeronautics, Northwestern Polytechnical University, Xi'an, 710072, China

(Manuscript Received April 17, 2018; Revised July 11, 2018; Accepted August 6, 2018)

Abstract

To have a better understanding of the unsteady aerodynamic characteristics of the airfoil which play important roles in wind turbine blade design, we investigated the boundary layer transition and separation on oscillating airfoil S809 using pressure signature captured in wind tunnel testing. The developed data processing technique of "sliding window" was applied to get useful transition and separation information. Meanwhile, the hysteresis effects of oscillation frequency on transition and separation were studied. It is found that (1) the root mean square (RMS) of pressure signature can indicate the transition and separation with the dimensionless window width of $\bar{m}$ = 0.0015; (2) the transitional attack of angle in up stroke is larger than that in down stroke at the state of the relative chord length of x/c ≥ 0.14, while the situation is opposite at the state of the relative chord length of x/c ≤ 0.14; (3) the flow separation is advanced and the reattachment is delayed with the increase of the oscillation frequency, which results in a greater hysteresis effect. The sliding window technique, whose parameters were determined in this paper, is effective for detecting boundary layer transition and separation from pressure signature.

Keywords: Pressure signature; Transition and separation; Sliding window; Hysteresis effect

1. Introduction

Wind turbines, helicopter rotor blades, jet engine compressor blades, and aircraft maneuverability etc. generally involve aerodynamic characteristics of pitching oscillation airfoil. The unsteady transition and separation flow in pitching oscillation airfoil should be carefully investigated. However, the current airfoil design methodologies still rely on steady computations and design criteria [1]. It is necessary to take the unsteady aerodynamic characteristics of the airfoil into account.

Among the unsteady boundary layer properties, boundary layer transition/relaminarization and separation/reattachment attract the researchers' attention especially.

Boundary layer transition generally results from a series of events, including instable waves, intermittent turbulent eddies, continuous turbulent eddies accompanied by increase in intermittency, sharp increase and rapid drop in turbulent intensity, and finally followed by fully-developed turbulence. At the same time, the increase in boundary layer thickness, surface temperature, wall shear stress and total pressure etc. become observable. It is convenient to define the peak of the root mean square (RMS) of temperature or pressure as indication of flow transition because of the ambiguous location of transition.

Dynamic stall, which has not been thoroughly studied, is an unsteady flow separation phenomenon. Carr [2] pointed out that the basic characteristics of dynamic stall are that there are complex unsteady separation and large-scale vortex structure in the flow field, and the aerodynamic force on the airfoil shows obvious nonlinear hysteresis. The flow separation and lift loss on the airfoil in the situation of dynamic stall are faster, more abrupt and more durable than that in the static situation. The development of the flow will have a great hysteresis in the dynamic stall process, which causes that the dynamic stall process is accompanied by large phase change of unsteady aerodynamic.

The main research methods of the dynamic aerodynamic characteristics on airfoil are numerical simulation and experimental research currently.

Numerical simulation of airfoil dynamic aerodynamic characteristics includes semi-empirical model based on experimental data and computational fluid dynamics (CFD) method, which are all imperfect methods. On one hand, some scholars have developed a series of semi-empirical dynamic stall models such as Leishman-Beddoes (L-B) model [3], ONERA model [4], Johnson model [5]. However, these models lack a deep understanding of the dynamic characteristic formation

*Corresponding author. Tel.: +86 13609249191
E-mail address: gyw630@nwpu.edu.cn
† Recommended by Associate Editor Hyoung-Bum Kim

mechanism and depend strongly on the application conditions. On the other hand, the common practice is unsteady numerical calculation based on the RANS equation [6-8]. Unfortunately, it reduces the reliability of numerical results due to the use of static transition prediction model and semi-empirical dynamic stall model.

Experimental research of airfoil dynamic aerodynamic characteristics has made some progress due to the development of experimental technology. In 1996, Pascazio et al. [9] studied the boundary layer dynamic development and the specific unsteady flow features such as transition and separation in pitching airfoils using the embedded laser velocimetry (ELV) method. They found that the transition delay occurrence could produce a significant modification of the turbulent boundary-layer behavior. The separation delay was shown to be more important than the reattachment delay when the reduced frequency k increases. In 2013, Marzabadi et al. [10] studied the effect of leading-edge roughness on the boundary layer of a plunging airfoil. They found that the surface roughness made the transition point move toward the leading edge and the laminar flow transited to turbulence as it passed over the roughness, and the turbulent boundary layer flow did not separate from the surface due to the oscillating energy of the boundary layer.

Commonly, the airfoil dynamic aerodynamic characteristics are studied by the experimental methods of the static airfoil for the lack of special methods for studying them.

In the static boundary layer transition detection tests, commonly used experimental methods have their own shortcomings, including hot wire method [8, 11-13], temperature sensitive paint method [14], infrared thermography [15], hot-film techniques [13] and flow visualization methods [16] and so on. Hot wire anemometry is an intrusive method that provides only point-wise flow information. Temperature sensitive paints should coat the model before tests. Infrared thermography and hot film sensors seem too complicated. In addition to the above, these techniques are not convenient for flight test or practical flow control. Therefore, it is still necessary to seek convenient, effective and practical transition detection methods for unsteady aerodynamics.

It is more convenient and practical for pressure transducers to detect boundary layer characteristics compared with the above experimental techniques. Early in 1970s, Helle [17] used acoustic technique to detect flow transition on hypersonic re-entry vehicles. Lews and Banner [18] investigated the boundary layer transition on the X-15 vertical fin using surface-pressure-fluctuation measurements. Due to the progress of technology of pressure transducer manufacture, the transducer rapid response and miniaturization have been improved greatly. The pressure transducer measurement technique for steady flow transition detection has now been applied to wide velocity range from low-speed flow to hypersonic in wind tunnel experiment.

There is little research on unsteady boundary transition on a pitching airfoil by using pressure signature, while the fluctuating pressure method has become mature in the static airfoil transition tests. In fact, the dynamic pressure time series can be used not only to calculate the dynamic aerodynamic force but also to analyze the transition and separation characteristics, which is ideal for the experimental study of the dynamic characteristics on airfoil. And we have done some research on unsteady boundary transition on a pitching airfoil by using pressure signature before. We used, the "phase average" method to study the transition characteristics of dynamic airfoils [19]. A very long sampling time, which was up to 20 minutes, was required hod. We developed a "slip window" method to study the dynamic airfoil characteristics, which is applied to the situation that there is only several periods' experimental data. The method of slip window uses the data collected in only one pitching cycle theoretically, so it does not take a long sampling time, which contributes to saving time in the experimental studies.

In this paper, the fluctuating pressure signature of the S809 airfoil in the pitching process was collected. The experimental data was processed by the slip window method developed in this paper. The effects of the oscillation frequency on the transition / relaminarization, separation / reattachment and the aerodynamic force were studied, which are useful in the aerodynamic design of wind turbine blades.

2. Experimental setup

The experiment was performed in the NF-3 wind tunnel at Northwestern Polytechnical University, Xi'an, China. NF-3 wind tunnel has three interchangeable test sections for low speed testing, i.e., airfoil test section, three-dimensional testing section and propeller test section. The size of airfoil test section is 8.0 m×1.6 m×3.0 m (length×height×width). The maximum wind speed is 130m/s, and turbulence intensity is less than 0.05 % in NF-3 wind tunnel.

The test model of airfoil S809 made of wood with steel skeleton inside was 500 mm chord length, 1600 mm span, and 21 % relative thickness. The airfoil model pitch axis was located at 1/4–chord. Nominal angle of attack angle was measured by angle sensor mounted on the pitch axis. The angle sensor was produced by HEIDENHAIN, German with resolution of ±5″. The model was driven by slider-crank mechanism as displayed in Fig. 1 in a sinusoidal motion of $\alpha = 8^{\circ} - 10^{\circ}\cos 2\pi ft$, where f was oscillation frequency.

Thirty XCQ-093 type of dynamic differential pressure transducers produced by Kulite, Inc., America were arranged on the upper and lower surface of the airfoil as displayed in Fig. 2. The diameter of the cylindrical probe of the sensor was 2.4 mm. These transducers were embedded in the test model and they were numbered clockwise from 1 to 30 starting at the trailing edge.

Agilent VXI system with 32 phases (Type E8401A) accomplished the dynamic data acquisition. The acquisition speed was 100 KHz/phase, acquisition frequency was 0~20 KHz, acquisition accuracy was 0.1 %, and cut-off fre-

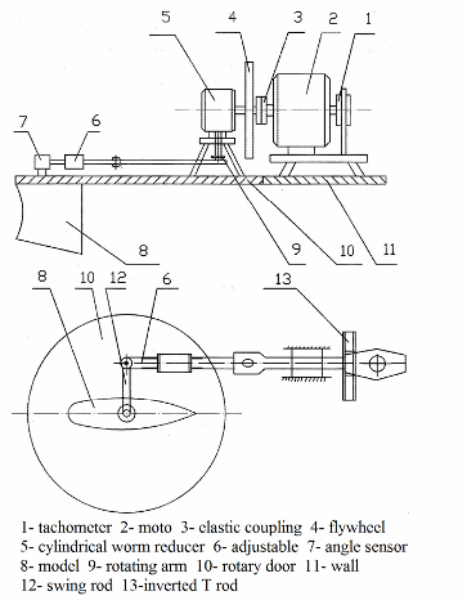

Fig. 1. Oscillation system and angle sensor.

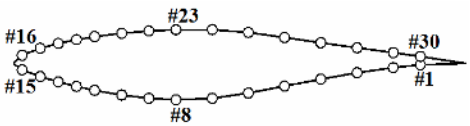

Fig. 2. Position and number of pressure transducers flush-mounted on the airfoil of S809.

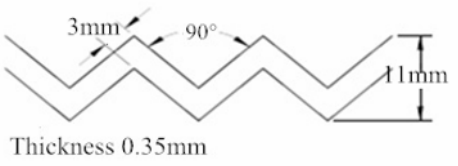

Fig. 3. ZZR type transition strip.

quency was 20 kHz.

The Reynolds number based on chord length was Re = 0.75×10^6 in the testing. The mean angle of attack was 8°. The oscillating amplitude was 10°. The oscillating frequencies were 0.5 Hz, 1.0 Hz and 1.5 Hz, corresponding to reduced frequencies of $k = 2\pi fc/U_\infty = 0.0785$, 0.1571 and 0.2356. Free transition test in wind tunnel was carried out for both static and oscillating airfoil. Fixed transition test was conducted only for oscillating airfoil. The zigzag transition strip of type ZZR (Fig. 3) was adhered to the upper surface of airfoil at the relative chord length of x/c = 0.05.

3. Data processing

3.1 Stationary airfoil

The Reynolds number for stationary airfoil was Re = 0.75×10^6 and the angle of attack was 8°. The sampling frequency was f_s = 10 kHz and sampling duration was 20 seconds. The averaged pressure of every sensor was calculated by

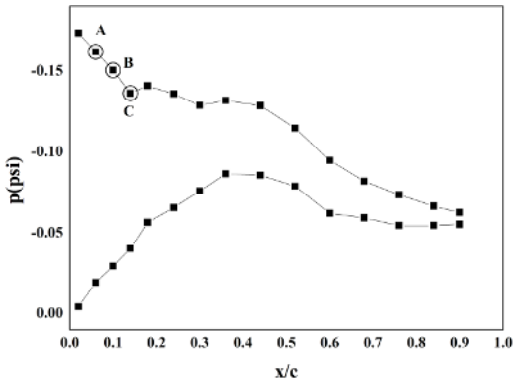

Fig. 4. Pressure distribution for stationary airfoil at Re = 0.75×10^6 and $\alpha = 8^o$.

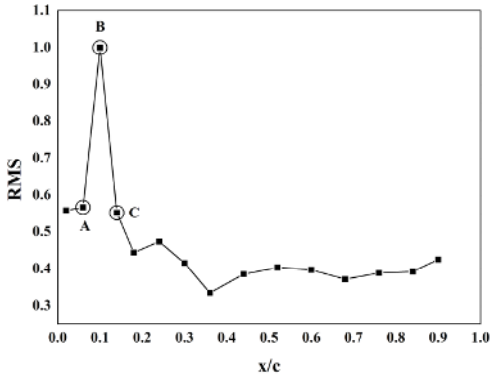

Fig. 5. RMS of pressure signature of sensors on the upper surface for stationary airfoil at Re = 0.75×10^6 and α=8°.

$$\overline{P}_i = \frac{1}{n}\sum_{j=1}^{n} P_i(t_j)\,, \tag{1}$$

and the RMS of pressure signature of the *i*-th sensor was calculated by

$$RMS_i = \sqrt{\sum_{i=1}^{n}(P_i - \overline{P})^2 \Big/ n}\,. \tag{2}$$

All calculated RMS were normalized by maximum RMS value.

The pressure distribution is displayed in Fig. 4. The pressure gradient on the upper surface is observable in the region of the relative chord length x/c = 0.02-0.14, covering the sensors A, B, C. Thus flow transition will happen in the region. The RMS at every sensor on the upper surface is shown in Fig. 5. The pressure RMS at sensor B is obviously larger than other sensors'. Therefore, it is reasonable to infer that sensor B should be in the transition region, or roughly speaking, the transition happens at the location of sensor B. The pressure signature at sensors A, B and C are displayed in Fig. 6, where the horizontal axis is the number of sampling points (25 milliseconds). It can be seen that the pressure signature at sensor B is more fluctuating, attributed to the superposition of turbulent

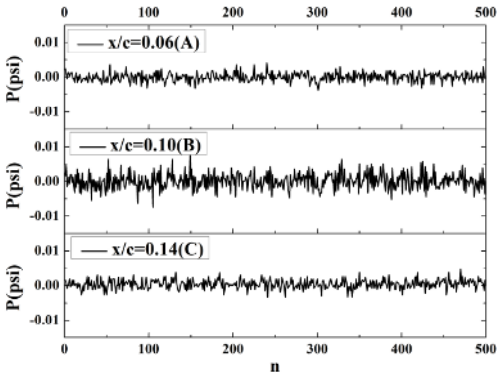

Fig. 6. Original pressure signature of sensors A, B and C for stationary airfoil at Re = 0.75×10^6 and α=8°.

pressure on basic laminar flow.

3.2 Oscillating airfoil

In the Ref. [19], it has been confirmed that the RMS value of the fluctuating pressure can characterize the transition features in the airfoil dynamic test. Therefore, the RMS value of the fluctuating pressure is still used to characterize the transition and separation features in this paper.

The Reynolds number for oscillating airfoil was also Re = 0.75×10^6. The mean angle of attack was 8° and the oscillation amplitude was 10°. The sampling frequency was f_s = 10 kHz and sampling duration was 20 seconds. The oscillation frequencies were 0.5 Hz, 1.0 Hz, 1.5 Hz, respectively, corresponding to the reduced frequencies of $k = 0.0785$, 0.1571 and 0.2356.

The phase-averaged method is often applied to the oscillating airfoil test. The phase-averaged method calculates the average pressure and RMS as the following expressions

$$\overline{p}_i = \frac{1}{n}\sum_{j=0}^{n-1} p(t_i + jT), \tag{3}$$

and

$$RMS_i = \sqrt{\frac{1}{n}\sum_{j=0}^{n-1}\left(p(t_i + jT) - \overline{p}_i\right)^2}, \tag{4}$$

where $T = 1/f$ is oscillation period, n is number of oscillation periods. As a general rule of thumb, 120 periods or so would give convergent mean and RMS values. However, as in the present test, the maximum number of oscillation periods was $20\times1.5 = 30$, far less than the required number, and so the mean and RMS values were not convergent.

Sliding window technique was employed in the present testing. A window is applied to truncate testing data and RMS values are calculated in term of the window data as the following formulas

$$\overline{p}_i = \frac{1}{2m+1}\sum_{j=-m}^{m} p(t_i + j\Delta t_s), \tag{5}$$

and

$$RMS_i = \sqrt{\sum_{j=-m}^{m}\left[W(t_i + j\Delta t_s)\,p(t_i + j\Delta t_s) - \overline{p}_i\right]^2 \Big/ (2m+1)}, \tag{6}$$

where $W(t)$ is symmetrical window function, Δt_s is sampling period, the reciprocal of sampling frequency f_s, $2m+1$ is window width.

Varieties of window functions can be chosen, such as rectangle window and triangle window. Rectangle window was the first chosen because of its simplicity $W(t) = 1$. The effect of the width of rectangle window on RMS of pressure signature was investigated and displayed in Fig. 7. The original pressure signature was obtained from the sensor at the relative chord length x/c = 0.1 and the reduced frequency was k = 0.0785. Only results between 0.0 T and 0.4 T are displayed in Fig. 7 because the RMS of pressure signature of separation flow between 0.4 T and 0.7 T is too much higher than RMS of transition flow, so that the transition event is not easy to be identified on the same coordinate scale.

In Fig. 7, with small window half width (m = 5), the variation of RMS is literally disorder, and it is difficult to recognize a transition event if it is not impossible. However, the widened window discloses transition event hiding in the pressure signature. The window width of m = 30, 50 obviously makes the transition peak prominent. However, the window technique could not precisely determine the instantaneous flow characteristics because the window technique introduces extra flow information from previous and following time moments.

For general oscillating airfoil of $\alpha = \alpha_0 + A\sin 2\pi ft$, the oscillating angular speed ω is

$$\omega = \frac{d\alpha}{dt} = 2\pi fA\cos(2\pi ft). \tag{7}$$

And the variation of α caused by discrete sampling with frequency f_s is

$$\Delta\alpha_s = \omega\cdot\Delta t = 2\pi fA\cos(2\pi ft)/f_s. \tag{8}$$

So the variation of α caused by window width is

$$\Delta\alpha = 2m\Delta\alpha_s = 4m\pi Af / f_s\cos(2\pi ft). \tag{9}$$

Therefore, the more widened window (m) increases the uncertainty of angle of attack. Higher sampling frequency can decrease the uncertainty. For the present case in Fig. 7, the uncertainty of angle of attack is $\Delta\alpha \approx 0.133°$ for m = 30, A = 10°, f = 0.5 Hz, t = 0.25s and f_s = 10 kHz.

A dimensionless pulse strength INB is defined according to

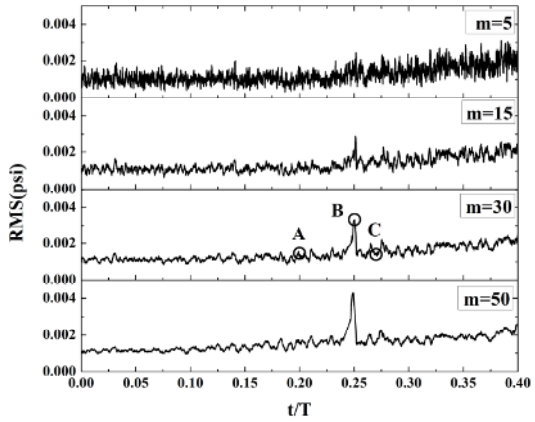

Fig. 7. Variation of RMS of pressure signature with rectangle window width at x/c = 0.1 and reduced frequency of k = 0.0785 (oscillation frequency of f = 0.5 Hz).

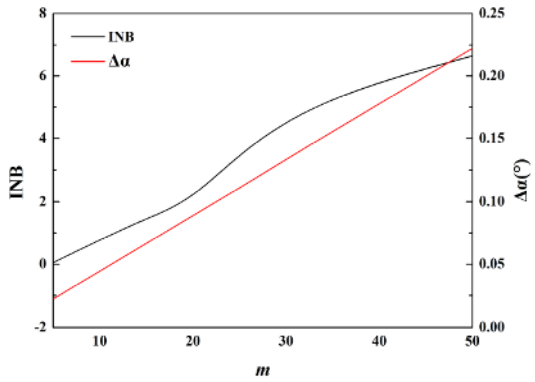

Fig. 8. Variation of INB and $\Delta\alpha$ with the half window width m.

the following equation to determine the window width in this paper.

$$INB_i = 20\log\frac{RMS_i}{RMS_N}, \tag{10}$$

where RMS_i is the i-th moment RMS value, and RMS_N is the mean RMS value in the i-th moment' deleted neighborhood with the size of 500 points.

Variation of INB and $\Delta\alpha$ with the half window width m is shown in the Fig. 8. This paper holds that the transition characteristic can be identified when $INB > 4$ combined with Figs. 7 and 8. And we chose the half window width of m = 30 in this paper considering that the uncertainty of angle of attack $\Delta\alpha$ cannot be too large.

A dimensionless window width $\overline{m}$ is defined according to the following equation in this paper.

$$\overline{m} = m\frac{f}{f_s}. \tag{11}$$

For the present case in Fig. 7, the dimensionless window width is $\overline{m} = 0.0015$ for m = 30, f = 0.5 Hz and f_s = 10 kHz. So the dimensionless window width determined in this paper

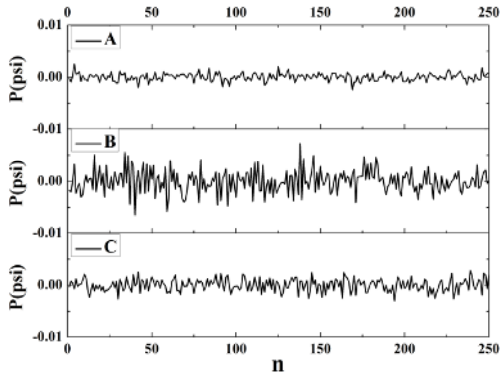

Fig. 9. Original pressure signature of time A, B and C.

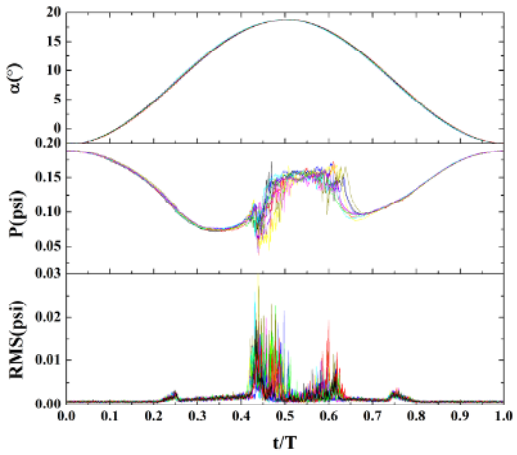

Fig. 10. Validation of effect of window technique on periodicity of mean and RMS values at x/c = 0.1 and reduced frequency of k = 0.0785.

is $\overline{m} = 0.0015$.

Although the reduced frequencies discussed in this paper are not high enough, the slip window method is still applied to the situation with high reduced frequency by increasing the sampling rate appropriately, according to Eq. (9).

The original pressure signature at times of A, B and C in Fig. 7 is displayed in Fig. 9 where the horizontal axis is the number of sampling points.

The pressure signature is similar to case of the stationary airfoil, but here, A, B and C are time instead of sensor locations. Both cases indicated that the RMS of pressure signature is closely related to flow transition event and can be used to determine the transition event.

Other window functions, such as Bartlett window, Hanning window, Hamming window, Blackman window, present the similar property as a rectangular window, but not shown here.

The effect of window function on periodicity of mean and RMS values of pressure signature was investigated as displayed in Fig. 10 by application of window technique ($\overline{m}$ = 0.0015) to data of 12 periods at x/c = 0.1 with the reduced frequency of k = 0.0785. The window-averaged pressure signatures of all 12 periods are nearly collapsed into a single

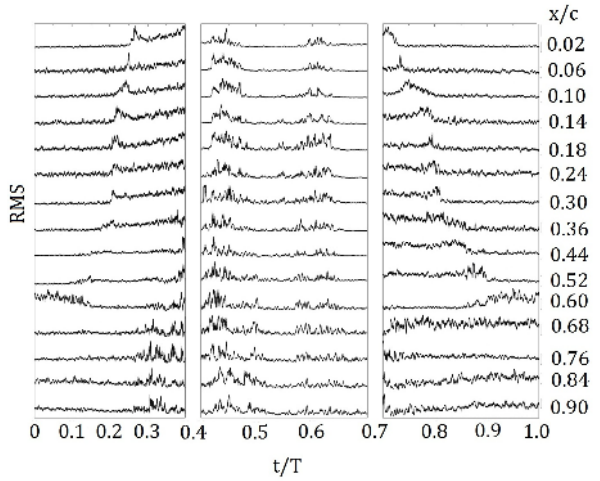

Fig. 11. Free transition case: RMS of pressure signature of sensors along chord. The RMS in the left and right subfigures was scaled to be easy visible.

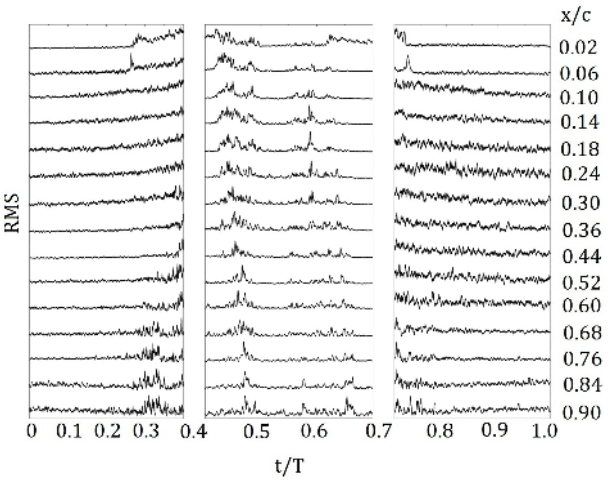

Fig. 12. Fixed transition case: RMS of pressure signature of sensors along chord. The RMS in the left and right subfigures was scaled to be easy visible.

curve except flow separation, which is really turbulent phenomenon. The RMS of window-averaged pressure signature of all 12 periods shows the transition peak at the same time.

4. Results and discussion

4.1 RMS of pressure signature for free and fixed transition on oscillating airfoil

The RMS of pressure signature of all 15 sensors on the upper surface along the chord for free and fixed transition are, respectively, displayed in Figs. 11 and 12 with the reduced frequency of $k = 0.0785$. The whole periodicity is divided into three parts because the RMS of separated flow overwhelms that of attached flow; therefore, the RMS of attached flow is scaled up, corresponding to 0 ~ 0.4 T (–2°~16°) and 0.7~1.0 T (11°~ – 2°).

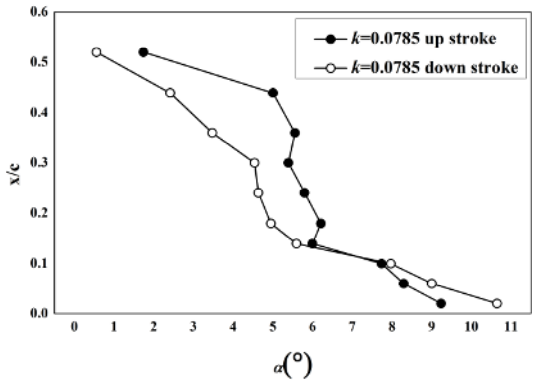

Fig. 13. Variation of transition and re-laminarization position for reduced frequency of $k = 0.0785$.

In the case of free transition, pitching-up motion promotes the flow transition from about x/c = 0.36 to x/c = 0.02 and pitching-down motion relaminarizes the flow from x/c = 0.02 to x/c = 0.52. The asymmetry implies hysteresis phenomenon. At the moment of t = 0.25 T (α=8°), the flow on almost the entire upper surface is turbulent. At the moment of t = 0.4 T (α=16°), the flow begins to separate. Between 0.4 T~0.7 T, flow separation and attachment are observable.

In the case of fixed transition, the transition strip is adhered to the upper surface of airfoil at x/c = 0.05 between sensor at x/c = 0.02 and sensor at x/c = 0.06. No obvious transition peaks are observed downstream of sensors at x/c = 0.06, which means that the transition strip takes effect and turns flow into turbulence.

4.2 Transition and relaminarization

The variation of transition and relaminarization positions on the upper surface for the reduced frequency of $k = 0.0785$ are displayed in Fig. 13. The pitching-up moves transition position forward and the pitching-down moves relaminarization position backward. However, the hysteresis of transition and relaminarization is obvious. The moment of transition is ahead of that of relaminarization for x/c greater than 0.14. In the neighborhood of leading edge, the pitching-down facilitates flow relaminarization more quickly. In this paper, the intersection point of the transition and relaminarization is $\alpha \approx 7°$.

The effect of reduced frequency on transition and relaminarization is shown in Figs. 14 and 15. In the up stroke, the transition position moves from $x/c = 0.44$ to $x/c = 0.18$ rapidly during the time of $t/T \approx 0.2 \sim 0.218$ ($\alpha \approx 5°$~$6.17°$). In the down stroke, the relaminarization position moves from $x/c = 0.18$ to $x/c = 0.36$ rapidly during the time of $t/T \approx 0.8 \sim 0.82$ ($\alpha \approx 4.64°$~$3.41°$) similar to the situation in up stroke. In this paper, the reduced frequency has a greater effect on the relaminarization in the down stroke than that on the transition in up stroke. The initial attack angle of the relaminarization increases from $\alpha = 10.56°$ to $\alpha = 14.3°$ with the reduced frequency increases from $k = 0.0785$ to $k = 0.2356$. This will lead to the shortened turbulence duration in down

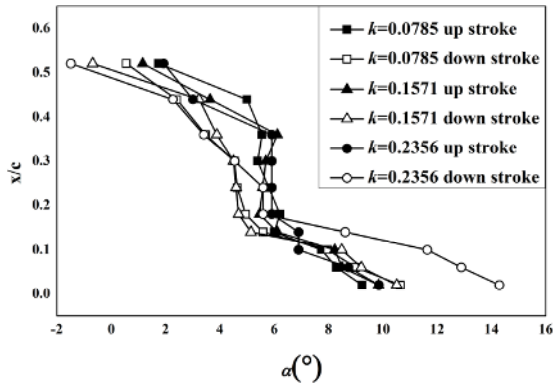

Fig. 14. Hysteresis effect of the transition/relaminarization.

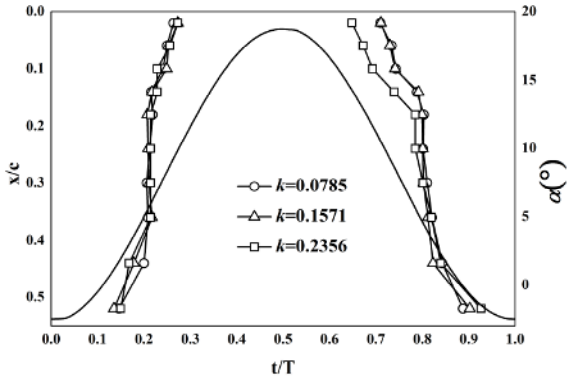

Fig. 15. Effect of reduced frequency on transition and re-laminarization.

stroke on the airfoil leading edge.

4.3 Separation and reattachment

As displayed in Fig. 16, a large RMS value occurs between 0.4T~0.7T, corresponding to angles of attack of 16°~18° , which should be in the stall state. The pressure distributions (relative to atmospheric pressure) on the upper surface at time C, D, E and F are present in Fig. 17. From time C to time D, the angle of attack is increasing, and the adverse pressure gradient gets strengthened. At time E and F, the pressure distributions indicate obvious pressure plateau, meaning large scale flow separation. The original pressure signature at time B and D is compared in Fig. 18 where time B refers to transition state and time D refers to separated state and the duration time is 250 milliseconds. Obviously, the pressure signature at time D in the separated state is much more fluctuated than that at time B in the transition state. These evidences demonstrate that not only can the RMS variation of pressure signature determine the flow transition, but also identify the flow separation.

The separation time here is defined as the time when the first large RMS occurs in relation to transition peak, and similarly the reattachment time is defined as the time when the last large RMS occurs in relation to relaminarization peak. In

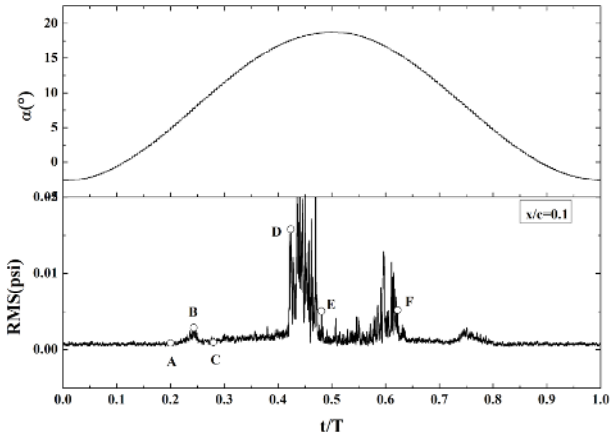

Fig. 16. Variation of RMS with time at x/c = 0.1 and k = 0.0785.

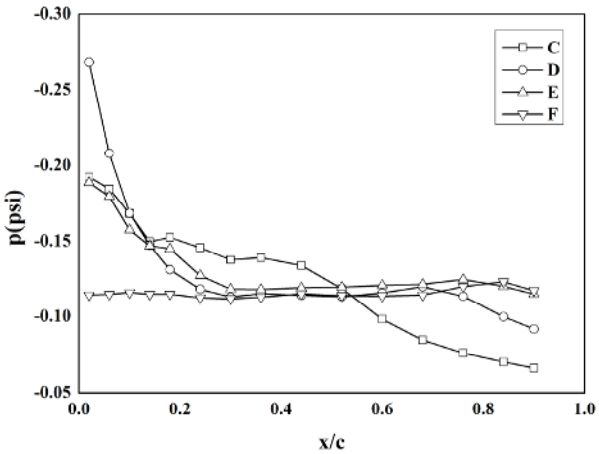

Fig. 17. Pressure distribution on the upper surface.

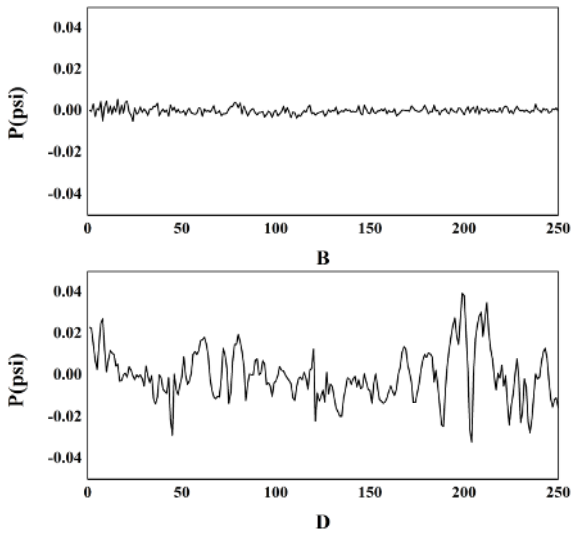

Fig. 18. Comparison of pressure signature between time B and D.

terms of the definition, the times D and F in Fig. 15 correspond to separation and reattachment, respectively. In terms of the definition, the effect of reduced frequency on separation

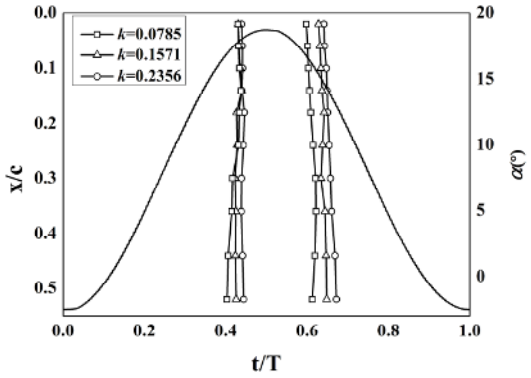

Fig. 19. Effect of reduced frequency on flow separation and reattachment.

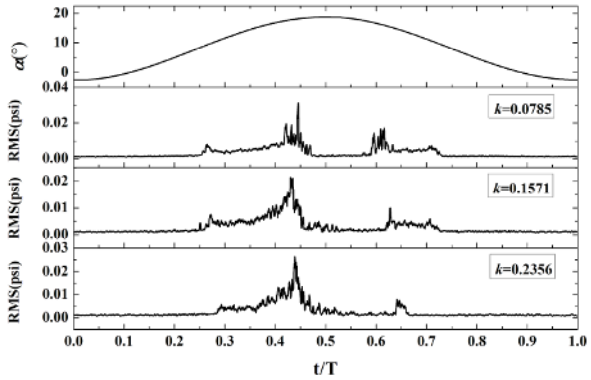

Fig. 20. Comparasion of RMS at x/c = 0.02 for different reduced frequency.

and reattachment on the upper surface is investigated in Fig. 19, which displays variation of position of separation and reattachment with time. The separation position moves forward in up-stroke and reattachment position moves backward in down-stroke. The flow separation in the pitching-up motion develops more quickly in relation to flow reattachment in the pitching-down motion, as the slope of $(dx/c)/(dt/T)$ indicated in Fig. 19. Both flow separation and reattachment are accelerated with the increase of reduced frequency as reflected in Fig. 18 in that the lines of *x/c* vs. *t/T* are more inclined to the right with increasing in reduced frequency. And with the reduced frequency increases from $k = 0.0785$ to $k = 0.2356$, the flow separation and reattachment time delay about $\Delta(t/T) = 0.041$ and $\Delta(t/T) = 0.0594$ respectively, corresponding to the flow separation angle of attack increasing by $\Delta\alpha \approx 1.282°$ and the flow reattachment angle of attack decreasing by $\Delta\alpha \approx 3.211°$.

The asymmetry of separation and reattachment at x/c = 0.02 is also present in RMS variation as Fig. 20 displays. With the change of reduced frequency, the transition and the separation time of the airfoil leading edge are almost unchanged, while the reattachment and relaminarization time in the down stroke are obviously different. With the reduced frequency increasing, the time of flow attached delays (attack angle gets smaller)

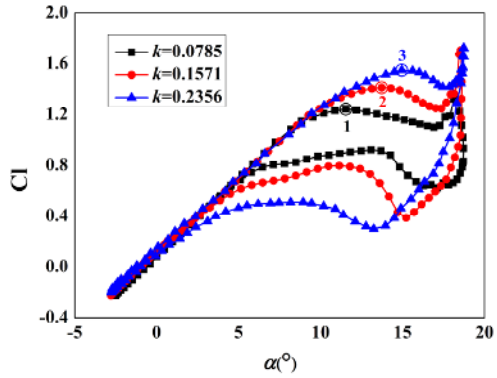

Fig. 21. Lift coefficient at different reduced frequencies.

and the relaminarization time move ahead (attack angle becomes larger). There is reason to believe that the flow directly attaches to the laminar flow if the reduced frequency further increases.

The asymmetry implies that the flow attachment duration in the pitching-up motion is longer than in the pitching-down motion, which leads to the large hysteresis near stall angles.

4.4 Aerodynamic force hysteresis features of pitching airfoil

The aerodynamic force of the airfoil shows a significant hysteresis effect in the experiment of pitching oscillation airfoil.

Fig. 21 shows the lift coefficient curves under the reduced frequency of $k = 0.0785$, $k = 0.1571$, $k = 0.2356$, which shows a significant hysteresis effect. As shown in Secs. 4.2 and 4.3, there is a hysteresis effect between transition / relaminarization and separation / reattachment, and the hysteresis effect of aerodynamic force results from the mutual aspects.

In the case of small angle of attack ($\alpha < 7°$), the hysteresis effect of transition/ relaminarization plays a role in the hysteresis effect of the aerodynamic force. It is known from Sec. 4.2 that the reduced frequency has a little effect on the transition in up stroke, and the effect on the relaminarization in down stroke is more significant. These lead to the fact that the reduced frequency in the range of the attack angle has a little effect on the lift coefficient in up stroke, and the effect in the down stroke is more significant.

In the case of large angle of attack ($\alpha > 7°$), the hysteresis effect of separation/ reattachment plays a great role in the hysteresis effect of the aerodynamic force. It is known from Sec. 4.3 that the hysteresis effect of separation/reattachment is gradually enhanced with the reduced frequency increasing and flow attachment duration in the pitching-up motion is longer than that in the pitching-down motion. This results in that the hysteresis loop of the lift coefficient becomes larger with the reduced frequency increasing in the situation of high attack angle ($\alpha > 7°$) in Fig. 21.

The variation curves of the lift coefficient Cl and the angle of attack of the point 1, 2 and 3 (the stall angle of attack) in Fig. 21 with the reduced frequency are shown in Fig. 22 to

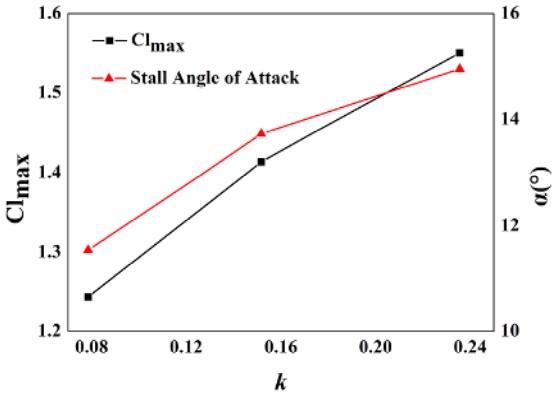

Fig. 22. Variations of the Cl_{max} and the stall angle of attack with reduced frequency.

better illustrate the hysteresis feature of Cl. As shown in Fig. 22, the Cl_{max} increases from 1.24 to 1.55 and the stall angle of attack increases from 11.54° to 14.95° as the reduced frequency increases from k = 0.0785 to k = 0.2356. The hysteresis effect of Cl increases with the reduced frequency increasing within the scope of this study.

5. Conclusions

The transition and separation events on oscillating airfoil S809 were investigated using pressure signature in this paper. The RMS of pressure signature was used to characterize the transition and separation in the present investigation. Sliding window technique developed here was applied to extracting useful transition and separation information.

In the case of fixed transition, no obvious transition peaks were observed downstream of the roughness, which means that the transition strip takes effect and turns flow into turbulence.

Transition/relaminarization shows a significant hysteresis effect. The transitional attack of angle in the up stroke is larger than that in the down stroke at the state of the relative chord length of x/c ≥ 0.14, while the situation is opposite at the state of the relative chord length of x/c ≤ 0.14. Separation / reattachment also shows an obvious hysteresis effect. And the effect of the reduced frequency is obvious. The flow separation is advanced and the reattachment is delayed with the reduced frequency increasing, which results in a greater hysteresis effect.

During the pitching oscillation of the airfoil, the mechanisms of flow transition / relaminarization and separation / reattachment are different. In the case of small angle of attack, the hysteresis of aerodynamic force is mainly due to the hysteresis effect of transition/ relaminarization, while in the case of large angle of attack, the hysteresis of aerodynamic force mainly depends on the hysteresis effect of separation/ reattachment.

And the hysteresis effect of Cl increases with the oscillation frequency increasing within the scope of this study. The Cl_{max} increases from 1.24 to 1.55 and the stall angle of attack increases from 11.54° to 14.95° as the reduced frequency increases from k = 0.0785 to k = 0.2356.

Acknowledgments

Thanks to all the staff in the NF-3 lab very much for their hard work and help in the wind tunnel experiment.

Nomenclature

α	: Angle of attack (°)
A	: Amplitude of the pitch oscillation (°)
f	: Frequency of the pitch oscillation (Hz)
f_s	: Sampling frequency (Hz)
k	: Reduced frequency
t	: Time (s)
Re	: Reynolds number (-)
c	: Chord length (m)
U_∞	: Free flow velocity (m/s)
$\overline{P_i}$	: Average pressure of the i-th pressure hole in stationary airfoil (psi)
P_i	: Pressure time sequence of the i-th pressure hole in stationary airfoil (psi)
RMS	: Root mean square value of the fluctuating pressure (psi)
INB	: Dimensionless pulse strength (-)
n	: Number of sampling (-)
T	: Oscillation period (s)
$\overline{p}_i$	: Average pressure of the i-th time or window in oscillating airfoil (psi)
m	: Half window width (-)
$\overline{m}$	: Dimensionless window width(-)
$W(t)$	: Window function (-)
Δt_s	: Sampling period (s)
$\Delta\alpha$	: Variation of α caused by window width (°)

References

[1] A. Klein et al., Unsteady criteria for rotor blade airfoil design, *35th European Rotorcraft Forum*, Hamburg, Germany (2009).

[2] L. W. Carr, Progress in analysis and prediction of dynamic stall, *J. of Aircraft*, 25 (1) (1988) 6-17, Doi: 10.2514/3.45534.

[3] J. Leishman, Validation of approximate indicial aerodynamic functions for two-dimensional subsonic flow, *J. of Aircraft*, 25 (10) (1988) 914-922, Doi: 10.2514/3.45680.

[4] K. W. Mcalister, O. Lambert and D. Petot, Application of the ONERA model of dynamic stall, *NASA TP-2399* (1984).

[5] M. Dindar and U. Kaynak, Effect of turbulence modeling on dynamic stall of a NACA0012 airfoil, *Aerospace Sciences Meeting and Exhibit* (1992).

[6] A. Jameson, Time dependent calculations using multigrid, with applications to unsteady flows past airfoils and wings, *Computational Fluid Dynamics Conference* (1991) Doi: 10.2514/6.1991-1596.

[7] S. Ko and W. J. Mccroskey, Computations of unsteady sepa-

rating flows over an oscillating airfoil, *Aiaa J.*, 35 (7) (1997) 1235-1238, Doi: 10.2514/2.226.

[8] T. Lee and P. Gerontakos, Investigation of flow over an oscillating airfoil, *J. of Fluid Mechanics*, 512 (512) (2004) 313-341, Doi: 10.1017/S0022112004009851.

[9] M. Pascazio et al., Unsteady boundary-layer measurement on oscillating airfoils - Transition and separation phenomena in pitching motion, *Aerospace Sciences Meeting and Exhibit* (1996) Doi: 10.2514/6.1996-35.

[10] F. R. Marzabadi and M. R. Soltani, Effect of leading-edge roughness on boundary layer transition of an oscillating airfoil, *Scientia Iranica*, 20 (3) (2013) 508-515.

[11] C. F. Knapp and P. J. Roache, A combined visual and hot-wire anemometer investigation of boundary-layer transition, *AIAA Journal,* 6 (1968) 29-36, Doi 10.2514/3.4437.

[12] J. E. Lagraff, Observations of hypersonic boundary-layer transition using hot wire anemometry, *AIAA Journal,* 10 (1972) 762-769, Doi: 10.2514/3.50208.

[13] K. Richter et al., Experimental investigation of unsteady transition on a pitching rotor blade airfoil, *J. of the American Helicopter Society*, 59 (1) (2014) 1-12, Doi: 10.4050/JAHS.59.012001.

[14] M. Costantini, U. Fey, U. Henne and C. Klein, Nonadiabatic surface effects on transition measurements using temperature-sensitive paints, *AIAA J.,* 53 (2015) 1172-1187, Doi: 10.2514/1.J053155.

[15] R. H. M. Giepman, F. F. J. Schrijer and B. W. van Oudheusden, Infrared thermography measurements on a moving boundary-layer transition front in supersonic flow, *AIAA J.* (2015) 1-5, Doi: 10.2514/1.J053910.

[16] E. Schülein, H. Rosemann and S. Schaber, Transition detection and skin friction measurements on rotating propeller blades, Paper AIAA-2012-3202, *28th AIAA Aerodynamic Measurement Technology, Ground Testing and Flight Testing Conference,* New Orleans, Louisiana, 25-28 June (2012) Doi: 10.2514/6.2012-3202.

[17] H. H. Heller, Acoustic technique for detection of flow transition on hypersonic re-entry vehicles, *AIAA J.,* 7 (1969) 2227-2232, Doi: 10.2514/3.5520.

[18] T. L. Lewis and R. D. Banner, Boundary layer transition detection on the X-15 vertical fin using surface-pressure-fluctuation measurements, *NASA TM X-2466* (1971).

[19] Y. Gao, Q. Zhu and L. Wang, Measurement of unsteady transition on a pitching airfoil using dynamic pressure sensors, *J. of Mechanical Science and Technology*, 30 (10) (2016) 4571-4578, Doi: 10.1007/s12206-016-0928-5.

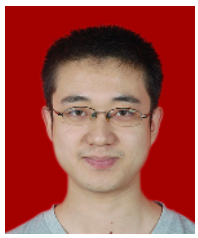

Binbin Wei received his Bachelor's degree in aircraft design, and Master's in fluid dynamics from Northwestern Polytechnical University (NPU) in China. He is currently studying for a Ph.D. in fluid dynamics at Northwestern Polytechnical University.

Yongwei Gao received his Bachelor's degree in aerodynamics, and Master's and Ph.D. in fluid dynamics from Northwestern Polytechnical University (NPU) in China. He is a Professor at the School of Aeronautics and head of the laboratory of NF-3 low-speed wind tunnel in NPU. His works focus on experimental fluid dynamics and aero acoustics.